Université Paul Sabatier - Toulouse III

Master 2 Recherche , spécialité Astrophysique, Sciences de L'Espace, Planétologie

Institut de Recherche en Astrophysique et Planétologie, Toulouse, France

MUSE integral field unit observation of the compact objects in the globular cluster NGC 6397

Author:
Manuel Pichardo Marcano

Supervisor:
Dr. Natalie Webb
Dr. Sebastien Guillot

Feb 1, 2016 - June 1, 2016

Co-funded by the Erasmus+ Programme of the European Union

Abstract

Globular clusters are very old groups of stars. Due to their age and the gravitational interactions dominating the dynamics of the clusters, they are home to a significant fraction of compact binaries. The formation and evolution of these kinds of binaries is still not completely understood. Of special interest is the globular cluster NGC 6397 as it is the closest core-collapsed cluster and has therefore been extensively studied with instruments like the Chandra X-ray Observatory, the Hubble Space Telescope, and more recently in the optical with the Multi Unit Spectroscopic Explorer (MUSE), installed on the Very Large Telescope (VLT). Integral field spectrographs, like MUSE, have many advantages compared to traditional long slit spectroscopic instrument, as spectra are obtained for every pixel and thus for every object in the large field of view ($1' \times 1'$). Here we present an analysis of the compact binary population in NGC 6397 taken with MUSE. The goal is to further understand the characteristics of the proposed bimodal population of cataclysmic variables (CVs) in the cluster, which have been suggested to be of primordial and dynamically formed origins. In this work we were able to spectrocopically confirm two new CV candidates as well as retrieve the spectra of three previously identified CVs. Spectral analysises of the extracted spectra allow us to estimate the mass ratio for a sample of the identified CVs. We also were able to compare the magnitude in the R band with previous observation of NGC 6397 to determine if any of the CVs were observed during an outburst. From the spectral emission and absorption lines we were also able to estimate the possible type of the companion and examine the magnetic nature of the CVs. We specifically searched for Helium II lines as signature of magnetism, and Titanium Oxide lines from a M type companion. We show that this shallow observation of NGC 6397 with MUSE is a good starting point to finally obtain optical spectra of compact objects in globular clusters but that with deeper observations a more complete study of the CVs and other compact objects can be carried out.

Acknowledgement

I would like to thank my two supervisors Dr. Natalie Webb and Dr. Sebastien Guillot, without their guidance and support this project would not have been possible.

I am also very grateful to everyone part of the compact object group at IRAP. I am specially grateful to Dr. Mickael Coriat and my office mate Mathias Peault.

I would also like to thank Dr. Victoria Barabash. Her comments and suggestion were welcomed and useful.

Disclamer: This project has been funded with support from the European Commission. This publication [communication] reflects the views only of the author, and the Commission cannot be held responsible for any use which may be made of the information contained therein.

Contents

List of Figures

List of Tables

Chapter 1: Introduction

1.1 Location, Location, Location

Important in real estate, but also seemingly an important factor to take into account when studying compact objects in binary systems. It seems that, like with people, where you were born plays a role in your evolution. This seems to be true for cataclysmic variables (CVs), the kind of compact binary system that we will explore in more detail in the present work. Our goal is to try to understand the formation of these kinds of systems when they are formed in a crowded and high density environment (like in a cluster of stars), and when you give them enough time to evolve and interact with other stars (like in a globular cluster).

Now that we have defined our broad goal, let us take a step back and explore in more detail what are compact objects, their different types, and the different ways they can interact with each other and other types of stars (Section. 1.2). That section will lead us to the discussion of where and how we expect to find them, and what can we learn by studying them in the different environments where they form (Sections 1.4).

1.2 Compact Objects or Stellar remnants

Compact objects, as their name suggest, are very massive and dense objects formed from the remains of a dying stars; hence their other name, 'stellar remnants'. They come in three main flavors, each following a different formation mechanism that is mainly determined by the mass of the progenitor star (de Boer & Seggewiss, 2008). The different types are neutron stars (NS), black holes (BH), and white dwarfs (WD) (see Sections 1.2.1,1.2.2 and 1.2.3). Besides these three, other possible exotic types of stars have been proposed; including quark stars, boson stars, and Thorne-Zytkow objects. These will not be discussed in this work as there is still a lack of observational evidence concerning their existence. The reader is referred to Madsen (1999) to discover more about these particular kind of proposed stars.

Of the three confirmed compact objects (neutron stars, white dwarfs and black holes), we will focus on the first two (NS and WD). They belong to a class of objects called "degenerate objects". These are objects for which the supporting force comes from the degeneracy pressure of fermions[1]. In the case of a white dwarf the pressure is provided by the degenerate electron gas (Fowler, 1926), and for a neutron stars, the neutrons cause the repulsive pressure (Oppenheimer & Volkoff, 1939).

The next subsection will list some of the characteristics of NS, and WD (both when they are found in isolation (Sections 1.2.1 and 1.2.2) or in a binary system (Section 1.3). Black holes will be briefly discussed for the sake of completeness.

1.2.1 White Dwarfs

White dwarfs are the most common end product in the evolution of stars. Around 90% of stars will evolve to become WDs (Koester & Weidermann, 1980). This includes all main sequence stars[2] (MS) with a mass between ~ 0.6 and ~ 8 solar mass ($M_\odot$) (Koester & Chanmugam, 1990). The resulting white dwarf will have a mass between ~ 0.3 and ~ 1.4 $M_\odot$ (Prada Moroni & Straniero, 2009; Chandrasekhar, 1931), the

[1] Fermions are particles with half-integer spin. They follow the Fermi-Dirac statistics, thus obey the Pauli exclusion principle. The consequence of the exclusion principle is that two fermions cannot occupy the same quantum state. This is the origin of the degeneracy pressure.

[2] Main sequence stars are those that are burning hydrogen in their cores.

average mass being ~ 0.7 $M_\odot$ (Koester & Chanmugam, 1990). All this mass is contained in a radius of about ~ 0.01 $R_\odot$ (Kepler & Bradley, 1995). These are average values, but the mass-radius relation for a white dwarf is plotted in Figure 1.1. If we take the mean values mentioned before, this gives a mean density of 10^9 kg/m^3 . This mass-radius relation will be composition dependent and it depends, for example, on the element dominating the atmosphere composition (Hamada & Salpeter, 1961). About 80% of all white dwarfs have hydrogen-dominated atmospheres (spectral type DA), but there exists a second class where helium dominates the atmosphere composition (spectral types D0, DB, DC, DZ and DQ)(Wickramasinghe & Ferrario, 2000; Koester & Chanmugam, 1990). White dwarfs are also known to be magnetic. Surface magnetism ranges from about 10^5 to 10^9 G (Suh & Mathews, 2000). Isolated magnetic white dwarfs represent $\sim 5\%$ of all WDs. See Wickramasinghe & Ferrario (2000) for a review on magnetism in WDs and for more details on the physics of white dwarfs the reader is referred to Koester & Chanmugam (1990) and Kepler & Bradley (1995).

1.2.2 Neutron Stars

Neutron stars are produced from the gravitational collapse of a massive star (> 8 $M_\odot$)(de Boer & Seggewiss, 2008) at the end of its life. The type II supernova produced by this collapse, leaves behind a dense and massive core (~ 12 kilometers in radius de Boer & Seggewiss 2008), but up to ~ 2 $M_\odot$, this limit being model dependent (see Lattimer & Prakash 2007). For comparison with white dwarfs, a sample mass-radius relation for a NS (red) is plotted along with that of a white dwarf (blue) in Figure 1.1. Like WDs, neutron stars are also known to be magnetic. The range in their magnetic field being from $\sim 10^7 - 10^{13}$ G. There also exist some neutron stars with unusually strong magnetic fields (B $\sim 10^{14} - 10^{15}$ G) called "magnetars" (Duncan & Thompson, 1992). For a review on magnetic fields in neutron stars see Reisenegger et al. (2005).

Neutron stars are mainly composed of neutrons and a thin atmosphere of a few cm of hydrogen or helium (Zavlin et al., 1996). We have come a long way since the first proposition of their existence, but there is still a lot of uncertainty concerning their interiors and a lot of conflicting models are proposed (Lattimer & Prakash, 2007). Since we have had observational evidence on their existence (Hewish et al., 1968) efforts have been made to constrain the different models. Figure 1.2 shows a visual summary of some of the different models proposed. The list of existing theoretical models for the composition of the interior of a neutron star is vast. This includes models assuming a composition of normal matter as well as other more exotic models based on strange quark matter or pure strange quark matter. For normal matter, the Equation of State (EOS) is that of an interacting nucleon gas, were the pressure and energy density vanish at the surface of the star (Lattimer & Prakash, 2001). Neutron stars can also be composed of exotic matter, such as hyperons and quark matter (Madsen, 1999). All these models give a theoretical relation between the pressure (P) and the energy density of matter (ρ). These relation, $P(\rho)$, can be translated into a mass-radius relation $M = M(R)$. This is what is shown in Figure 1.2. The upper left and lower right regions of the Figure can be excluded on the basis of general relativity and other physical constraints. For a detailed discussion on the structure and the Equations of State of neutron stars the reader is referred to Lattimer & Prakash (2001). Accurately measuring the neutron star mass and radius would help constraint the EOS of neutron stars. One way of doing this is obtaining spectroscopic observation of neutron stars at a know distance (e.g., spectra of neutron stars in globular clusters).

1.2.3 Black Holes

Black holes are the fate of collapsing matter when no force, including the degeneracy pressure of neutrons, is enough to repel gravitational attraction. Black holes, like neutron stars and white dwarfs, can be the result of the collapse of a single main sequence star. Stars with an initial mass $\gtrsim 20$ $M_\odot$ can end their lives as a black hole (Heger et al., 2003), but the initial mass is not the only factor that comes into play. For

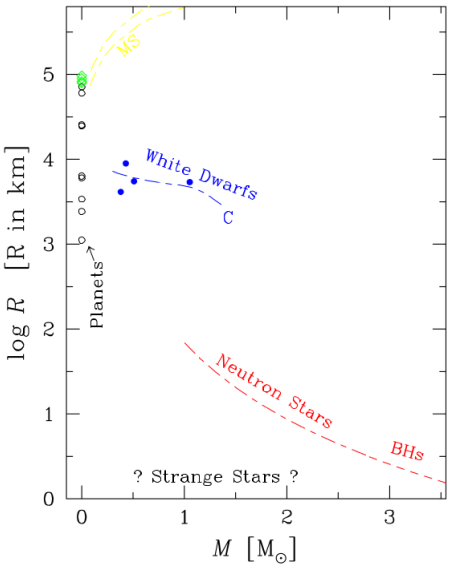

Figure 1.1: Mass-radius relation for different objects (de Boer & Seggewiss, 2008). The mass-radius relation is given by the specific Equation of State of the material in the interior. For the case of white dwarf and neutron star the interior is degenerate matter. Many models exist for the equation of state of these compact objects, specially for neutron stars, only one of such model for each object is presented in this figure.

example, the formation of the black hole will depend also on the metallicity of the star and/or binarity. See Heger et al. (2003) and Brown et al. (2000) for details on the evolution of high mass stars and the different formation paths leading to a black hole from a single collapse star.

To compare the physical characteristics of a black hole with other compact objects, we can define the gravitational radius or Schwarzschild radius of a black hole. This is the radius to which a given spherical and non-rotating mass needs to be reduced to get a escape velocity equal to the speed of light. This translates to:

$$r = \frac{2MG}{c^2} \tag{1.1}$$

An estimate of the lowest mass of a black hole is the maximum possible mass for a neutron star, this is $\sim 3M_\odot$ (Rhoades & Ruffini, 1974). With the formula above we can get a rough estimate on the size of a stellar mass black hole. A mass of 3 $M_\odot$ and the formula above gives an equivalent Schwarzschild radius of about 9 km.

1.3 Compact Binaries

Compact binaries are those binaries where at least one of their components is a compact object (WD, NS or BH). In this section we will start by discussing some of the basic concepts of binary evolution, followed by a discussion on mass exchange between binary components, and we will finish by looking in more detail at some specific examples of compact binaries that are relevant to this study.

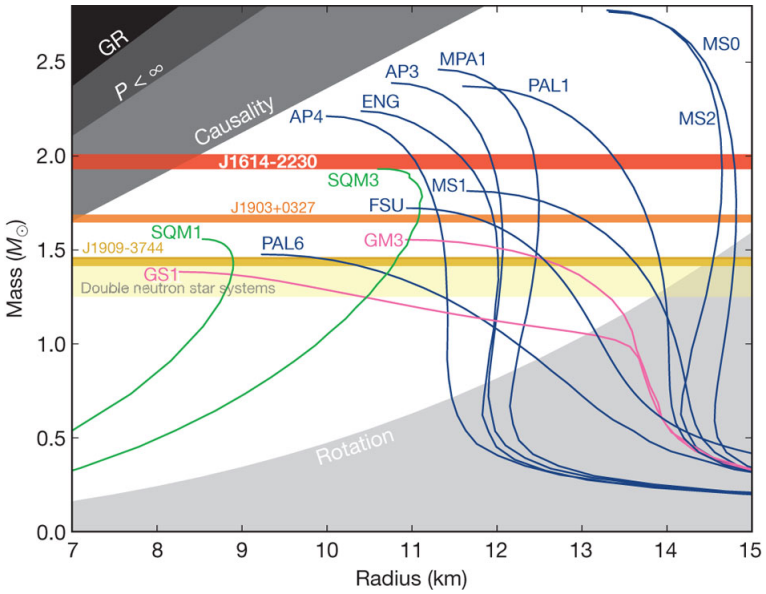

Figure 1.2: The plot shows non-rotating mass versus physical radius for several typical proposal model describing the interior of neutron stars. Blue, nucleons; pink, nucleons plus exotic matter; green, strange quark matter (Demorest et al., 2010).

1.3.1 The Gravitational Potential

The total potential of a binary system is the sum of the gravitational and the rotational potential. To get an analytical solution, we can assume a model in which the resulting disturbing potential is due to the presence of two point masses, M_1 (or the primary) and M_2 (the secondary). Moreover, we assume a co-rotating Cartesian reference frame (x,y,z) with origin at the primary M_1; whose x-axis is in the direction joining the two point masses; and the z-axis is perpendicular to the orbital plane. The total potential, Ψ at an arbitrary point P(x,y,z) then reads:

$$\Psi = -G\frac{M_1}{\sqrt{x^2+y^2+z^2}} - G\frac{M_2}{\sqrt{(R-x)^2+y^2+z^2}} - \frac{\omega^2}{2}\left[(x-\mu R)^2+y^2\right] \tag{1.2}$$

where G is the gravitational constant, R represents the separation between the point masses, and $\mu = M_2/(M_1+M_2)$. We further assume that the binary orbit is Keplerian, thus the orbital frequency is given by:

$$\omega^2 = G\frac{M_1+M_2}{R^3}/ \tag{1.3}$$

Taking into the account the assumptions mentioned above, the surfaces generated by Equation 1.2 are called *Roche Equipotential*[3]. Figure 1.3 show such equipotential surfaces (x,y plane). Of special interest are two regions on the graph:

- The inner Lagrangian point $\mathbf{L_1}$. This is where all the forces cancel out.
- Critical or **Roche lobe**. The surface that has the potential equal to the potential at L_1.

[3]We are neglecting here the radiation pressure from the stars. For more details on roche potentials including radiation Effects see Schuerman (1972)

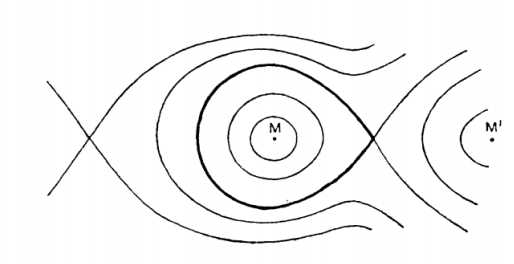

Figure 1.3: Geometry of the Roche surfaces. The Roche lobe for object M is marked in bold lines (Kopal, 1959).

The Roche lobe has the property that inside the lobe of an object, any material will be gravitationally bound to that object. With this knowledge we can classify binary systems into three groups:

1. **Detached systems**. If the volumes of both components are significantly smaller than their Roche lobe.
2. **Semi-detached systems**. Where one of the components fills its Roche lobe.
3. **Contact systems**. Where both components appear to fill their respective Roche lobes.

This classification scheme was first suggested by Kopal (1955) and developed in detail in a comprehensive monograph in 1959 (Kopal, 1959).

1.3.2 Binary Evolution

In this work we are mostly interested in the formation of semi-detached compact binary systems. In this section, we briefly explore a possible scenario for their formation.

These kinds of systems can be formed from two previously detached MS stars binaries that evolve on different timescales due to their different masses. This can be seen noticing that the luminosity, L, indicates the rate of consumption of nuclear fuel; and the nuclear fuel repository is proportional to the mass, M. This gives us a rough estimates of the nuclear timescale of a star given by:

$$\tau \propto \frac{M \times 6 \times 10^{18} \text{ erg g}^{-1}}{L}, \tag{1.4}$$

where L is the luminosity, M is the mass, and 6×10^{18}erg g^{-1} is the energy release fusing a gram of hydrogen to helium. Moreover, with the mass-luminosity relation $\mathrm{L}/\mathrm{L}_\odot = (M/\mathrm{M}_\odot)^\alpha$, where $\alpha \gtrsim 3$ (e.g. de Boer & Seggewiss, 2008), we can conclude that in a system starting with two detached main sequence stars, the more massive one will evolve beyond the main sequence faster. As it expands after it leaves the main sequence in the process of becoming a compact object, a common envelope around both stars will be formed. This allows the two stars to get close enough to interact. The envelope is then expelled, leaving behind a binary system with a compact object and an evolved main sequence star. The old main sequence star in the binary, as it continues to evolve, will expand and fill its Roche lobe, allowing for accretion into the compact object to happen. The process is more complex and, among other things, depends on the initial mass of both stars and initial binary separation. For example, a binary system starting with a 2 $\mathrm{M}_\odot$ and a 1 $\mathrm{M}_\odot$ star can produce a white dwarf accreting from a late-type main sequence star (Kippenhahn et al., 1967; De Loore & Doom, 1992). A system starting with a 15 $\mathrm{M}_\odot$ and 2 $\mathrm{M}_\odot$ will become a neutron star accreting from a low mass main sequence star (van den Heuvel, 1976). In the case of starting masses of

20 $M_\odot$ + 8 $M_\odot$ this can produce a neutron star (or black hole) accreting from a high mass main sequence star (van den Heuvel, 1976). The details on the evolution of close binaries can be found in Postnov & Yungelson (2014) and de Boer & Seggewiss (2008)

In the next section we will see in some detail how the accretion can take place once the compact binary is formed due to stellar evolution of their constituents.

1.3.3 Accretion

In the Roche overflow scenario we have incoming gas from the secondary star. After it passes through the L_1 point we assume a ballistic behavior completely dominated by the gravitational potential of the compact object. This is justified by the fact showed by Lubow & Shu (1975) that the stream is supersonic and we can ignore pressure. We can also assume that the incoming speed must be small. This is safe to assume if the accretion is due solely to overflow and thus the velocity is of the order of the sound speed in the atmosphere of the secondary star. This speed is much slower than the orbital speed of the binaries, and lower than the velocities acquired during the fall. This simplification means that we can treat the Roche lobe as a zero velocity surface. Meaning that the motion of the gas can be approximated as the trajectory of a test particle released from rest with an initial angular momentum from L_1. This creates an elliptical orbit of the stream around the primary star (Figure 1.4 a). As the gas flow continues, it will impact itself. This causes the flow to modify its orbit to that of the lowest energy at a specific angular momentum (we assume angular momentum is conserved). Of course the orbit of lowest energy at a given angular momentum is a circular one (see Figure 1.4 b). This creates a ring around the compact object. We can estimate the radius of this ring by invoking again the assumption that no angular momentum is lost in the process. The angular momentum at L_1 would be given by $R_{L1} \times V_{orbit}$ (where R_{L1} is the distance from the secondary to L_1). Knowing that $\omega = (2\pi)/\text{Period}$ and equating the angular momentum at L_1 to the angular momentum of a Keplerian orbit at R_{ring} we get:

$$\frac{R_{ring}}{R} = \left(\frac{R_{L1}}{R}\right)^{\frac{1}{4}} (1+q), \tag{1.5}$$

where q is the mass ratio ($q = \frac{M_2}{M_1}$), and I used Equation 1.3 to simplify the answer by canceling some constants. This is called the *circularization radius*. After a ring is formed (Figure 1.4 b), as first indicated in Lynden-Bell & Pringle (1974), any viscous processes will cause the ring to spread to conserve angular momentum (Figure 1.4 d). The nature of these viscous torques will not be discussed here. For a review on the topic see Frank et al. (2002) and Verbunt (1982). Roche lobe overflow is not the only type of accretion, others include wind accretion or Bondi accretion. In this work, unless otherwise stated, accretion will mean accretion by Roche lobe overflow. See the references cited above for more details on other types of accretion.

Now that we studied briefly accretion and saw how it can happen in semi-detached binaries, in the next section we will discuss two specific semi-detached systems: one where the accretion is onto a white dwarf (Cataclysmic Variable), and the other where the accretion is onto a neutron star or a black hole (X-Ray binaries).

1.3.4 Cataclysmic Variables

Cataclysmic variables (CVs) are semi-detached binary systems comprised of a white dwarf (primary star) and typically a low mass main sequence star. CVs are generally classified into two groups. Magnetic CVs ($\sim 10^6 - 10^8$ G) and non-magnetic CVs (B < 0.01 MG). Magnetic CVs constitute about 25% of the known CV population (Balman, 2012). CVs have typical periods in the range of 1-10 hrs. In this period range the distribution is not uniform. In fact, there is a well defined region (orbital period (P_{orb}) between 2.3 and 2.8 hours) where there is a deficiency of non-magnetic CVs. This is called the 'period gap'. CVs

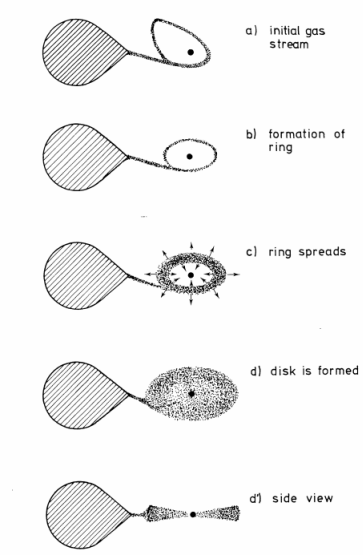

Figure 1.4: Schematic illustration of the formation of an accretion disk around a compact binary (Verbunt, 1982).

above the period gap are assumed to lose angular momentum via magnetic braking, and CVs below the period gap lose angular momentum purely by gravitational radiation. The magnetic braking stops when the secondary star becomes fully convective. At this point the accretion stops and the system becomes a detached one. Angular momentum is then lost solely via gravitational radiation. This shrinks the orbit and brings the two stars into contact resuming the mass transfer (e.g. Warner, 2003).

CVs can be observed in many wavelengths. This includes radio observation of jets (Körding et al. 2008,Coppejans et al. 2015), optical and ultraviolet observations of the accretion disks (Kinney, 1994), and X-rays ($\sim 0.5 - 2.5$ keV) from the infalling plasma onto the white dwarfs (Verbunt et al., 1997). As their name suggests these are very variable systems, specially the non-magnetic CVs. These variabilities are due either to instabilities in the accretion disk, referred to as dwarf novae (Osaki, 1974), or unstable burning of hydrogen at their surface, called nova (Starrfield et al., 2016). We will discuss the outburst caused by these instabilities, and the nature of the magnetic CVs by presenting the classification of CVs and exploring the taxonomy of these objects.

1.3.4.1 Classical Novae (CN)

When the surface of an accreting white dwarf becomes hot enough ($\sim 10^8$ K, e.g. Starrfield et al. (2016)), nuclear fusion can take place and a thermonuclear runaway happens. This creates a violent explosion capable of ejecting material (mean mass of $\sim 2 \times 10^{-4}$ $M_\odot$) at high velocities ($\sim 10^2 - 10^3$ km s^{-1}) (Gehrz et al., 1998; Shara, 1989). These outburst are fairly easy to detect since they cause a substantial increase in brightness (typically ~ 12 magnitudes in optical , Shara 1989). A CV observed erupting in such a way is classified as a *classical nova (CN)*. Classical novae are seen to erupt only once. If a previously recognized CN erupts again as a CN they are called recurrent novae.

1.3.4.2 Dwarf Novae (DN)

A dwarf nova outburst is caused by instabilities in the accretion disk. This is predicted to happened in non-magnetic CVs with low accretion rates (Osaki, 1974). CVs that show these outbursts are classified as dwarf novae. The outburst from a dwarf nova is not as violent as the one from a classical novae. The

magnitude increase is only of about 2-5, and no material is ejected. They also, unlike classical novae, are periodic in nature on times scales of weeks to years depending mainly on the accretion rate (Shara, 1989). Probably the best known example of a dwarf nova is the variable star SS Cygni (e.g. Cannizzo & Mattei, 1998, for a review).

1.3.4.3 Novae-like (NL)

CVs can also be classified as novae-like. They are CVs that seem to have stable accretion, thus not undergoing dwarf novae outburst and having a bright stable disk. They represent the 'non-eruptive' CVs.

1.3.4.4 Polars

Polars are CVs with a strong magnetic field. The value of the magnetic field is usually between 20 MG to 230 MG (Balman, 2012). The magnetic field in polars is so strong that it couples to the magnetic field of the donor and forces the WD to corotate with the companion. The presence of the strong magnetic field also disrupt the accretion disk. In the case of polars the accretion flow is channeled by the magnetic field lines onto the magnetic poles. This causes X-ray radiation (produced by shocks and bremsstrahlung radiation) and strongly circular polarized ($> 10\%$) cyclotron radiation in the optical and infrared bands (Cropper, 1990). This polarized emission is the reason for the name Polars (Krzeminski & Serkowski, 1977). The polarization was the first clue on the magnetic nature of these type of systems. It was first discovered for AM Herculis (AM Her), now the prototype polar CV (Tapia, 1977). Polar systems are often referred to as AM Her-like system. This kind of systems represent 63% of the magnetic CV population (Balman, 2012).

1.3.4.5 Intermediate Polars (IPs)

Intermediate polars are the second kind of magnetic CVs. In this class the magnetic field is weaker ($\sim 1 - 20MG$). The weaker strength of the magnetic fields means that the accretion disk is not entirely dominated by the magnetic field, and the system is asynchronous, so the WD does not corotate with the binary. This kind of systems represent 37% of the known magnetic CV population (Balman, 2012). An extensively studied member of this class is DQ Her. DQ Her is sometimes refer as a subclass of IPs (IPs with period $\lesssim 120$ s), or even as a synonym for IPs (Patterson, 1994; Warner, 2003).

1.3.5 X-Ray binaries

X-Ray binaries are a subclass of compact binaries where the accretor is either a neutron star or a black hole. They can be classified into two regimes depending on the type of the donor star. If the donor or secondary is a late-type star it is called a low-mass X-ray binary; if it is an early-type star they are called high-mass X-ray binaries.

1.3.5.1 Low-mass X-Ray Binaries

Low-mass X-ray binaries (LXMBs) are Roche-lobe overflow binary stars consisting of a neutron star or a black holes accreting from a low-mass ($\lesssim 1.5\mathrm{M}_\odot$) donor. The donor can be a main sequence star or even a white dwarf (Tauris & van den Heuvel, 2006).

In the case of a LMXB, since the accretor (NS or BH) has a higher mass than the white dwarf in a CV, the energy release in the accretion process is higher compared to the energy released in the CVs. This means that we get more powerful X-ray radiation from LMXB (up to ~ 10 keV) (Tauris & van den Heuvel, 2006). The period can range from 11 minutes to 17 days, and like CVs they can show magnetism ($\sim 10^9 \sim 10^{11}$G) (Tauris & van den Heuvel, 2006).

1.3.5.2 High-mass X-Ray Binaries

High-mass X-ray binaries (HMXB) are the second class of X-ray binaries. In the case of a HMXB, the donor star is a young early-type main sequence star. This usually means an O or B spectral type with a mass $> 10M_{\odot}$ (e.g. Tauris & van den Heuvel, 2006). Contrary to LMXBs the accretion is not entirely due to Roche overflow, it can be due to the high velocity winds produced by the donor star. And also unlike LMXBs, these systems tend to show stronger magnetic fields and stronger X-ray radiation (Tauris & van den Heuvel, 2006).

1.4 Globular Clusters

Globular clusters (GCs) are very old and dense gravitationally bound groups of stars. Their age is generally around 10 Gyr (Meylan & Heggie, 1997) and typically contain $\sim 10^6$ stars (Knigge, 2012). Due to their age, we expect to find compact objects, and the high density environment is ideal for the formation of compact binaries. If fact the formation of these binaries plays an important role in the evolution of globular clusters. Globular clusters are known to have a phase where their evolution is governed by the formation and dynamics of binaries in their cores. This is called the "binary burning" phase. In this phase the gravitational collapse in a GC can be balanced by energy produced via dynamical hardening of binaries (binaries become more strongly bound) in the core (e.g. Hut et al., 1992). The importance of this effect is far from being completely understood, and a better understanding on the compact binaries in GCs is needed. The search for these compact binaries have been effective leading to the detection of X-ray binaries and Cataclysmic Variables in some globular clusters (e.g. Maccarone & Knigge, 2007). Nonetheless, the formation and evolution of these kinds of binaries is still not completely understood, and many uncertainties remain. Of special interest for this project are the cataclysmic variables in globular clusters. In the next subsection, we will make a brief overview on the current knowledge on the subject and state the current open questions that we mean to address in this project.

1.4.1 CVs in Globular clusters

Cataclysmic Variables are tracers of the dynamical evolution in globular clusters. Their number and spatial distribution can give us a clue on the past of the globular cluster, and help us constrain models of stellar and dynamical evolution. CVs are expected to be the most abundant compact binary based on the fact that the white dwarf is the most common fate of stars. Theoretical modeling predicts ~ 100 CVs in a given GC (varying a bit with the cluster metallicity and stellar density, see Ivanova et al., 2006). They are expected to form two distinctive groups based on their formation mechanism, primordial CVs and dynamically formed CVs (e.g. Hut et al., 1992). Primordial are those CVs that formed from primordial binaries that didn't get destroyed through a physical collision in the cluster. The dynamically formed CVs are those formed via dynamical encounters with other members in the cluster. This includes tidal capture, exchange interactions and collision events. For example a dynamically formed CV can form through the tidal capture of a MS star by a WD, or by a system resulting from the collisions between a red giant and a MS star (Ivanova et al., 2006).

The problem with the theoretical picture described above is that hitherto there is no observational evidence of two distinct CV populations in globular clusters. The lack of detection of these two predicted populations raises the question: **Where are all the primordial CVs?** The number can be theoretically predicted ($\sim 37\%$ of all CVs in a GC, Ivanova et al. 2006), but we need observational evidence to constrain the theoretical models. The dense environment in which they form and the possibility that CVs are formed through dynamical interaction can result in a differentiation of the binary population from the galactic field population. For example, for the GCs CVs their period distribution is expected to be different from that of

a field population as in the field almost all CVs are primordial and not dynamically formed CVs (Ivanova et al., 2005). So the questions becomes. **What is the period distribution of CVs in Globlular Clusters?** In the Galactic field the period distribution has been well studied. The period of CVs in the field is governed by magnetic braking ($P_{orb} \gtrsim 3h$), and gravitational radiation ($P_{orb} \lesssim 2h$) (Robinson, 1983). The CV period distribution in GC is still not well understood mainly due to lack of observational data. There are only 15 CVs with known periods from a small sample of 5 globular clusters (Knigge, 2012). Another difference between fields and GC CVs that has been proposed is that CVs in GCs tend to be primarily magnetic in nature (Grindlay, 1999). This could explain the lack of observed dwarf novae outburst in CVs (Shara et al., 1996) and the high X-ray luminosity of GC CVs, compared to fields CVs (Verbunt et al., 1997). However data is scarce to support that argument and the questions remain: **Are globular clusters in CVs mainly magnetic in nature and where are all the dwarf novae?**

With these questions in mind, we studied in this project the population of Cataclysmic Variables in a nearby globular cluster, NGC 6397. The next section describes the most important characteristic of NGC 6397 and the previous studies done regarding its compact binary population.

1.4.2 NGC 6397

NGC 6397 is the closest (2.4 kpc) core collapse[4] globular cluster (Harris, 1996; McLaughlin & van der Marel, 2005) with center at RA(J2000): $17^h\,40^m\,42.09^s$ and Dec(J2000): $-53^\circ\,40'\,27.6$" (Harris, 1996). A globular cluster can be characterized by three main radii. These are the core radius (r_c), half-mass (or half-light) radius (r_h), and the tidal radius (r_t). The core radius is the distance at which the apparent surface luminosity has dropped by half, the half-mass radius is the radius of the sphere containing the innermost half of the mass, and finally the tidal radius is the distance at which the gravitational influence of the clusters extents. For NGC 6397 these values are: $r_c = 0.05'$, $r_h = 2.90'$ and $r_t = 15.81'$ (Harris, 1996).

Due to its proximity, NGC 6397 has been extensively studied at different wavelengths. The observation by Cool et al. (1993) with the ROSAT satellite was the first one to detect X-rays sources in NGC 6397. This was followed by a photometric study with the Hubble Space Telescope Wide Field and Planetary Camera (WFPC) confirming the first three CVs candidates in NGC 6397 (Cool et al., 1995). Since then follow-up observations with Chandra (Grindlay et al., 2001; Bogdanov et al., 2010) and with Hubble (Taylor et al., 2001; Grindlay, 2006), both with the Faint Object Spectrograph and with the Advanced Camera for Surveys (ACS), have found a total of 15 CVs candidates (Cohn et al., 2010). From these currently known candidates, only 4 have been spectroscopically confirmed (Grindlay et al., 1995; Edmonds et al., 1999), and the period is known for only two of them (Kaluzny & Thompson, 2003; Kaluzny et al., 2006).

In this work our goal is to exploit new data available from NGC 6397 and increase our understanding of CVs in globular clusters. We particularly try to extend the sample size of spectroscopically confirmed CVs and study their properties (e.g. period, mass and variability). In the next chapter, we will discuss the nature of the observations and data used for the analysis.

[4]Core collapse are clusters showing a power-law slope in their surface brightness profile near the center due to the gravothermal instability (Antonov, 1962; Lynden-Bell & Wood, 1968; Lynden-Bell & Eggleton, 1980). In contrast to other isothermal sphere models showing a more flatten brightness profile in the center (e.g. King, 1966)

Chapter 2: Observation and data reduction

2.1 VLT/MUSE

NGC 6397 was observed with the Multi Unit Spectroscopic Explorer (MUSE) at the Very Large Telescope (VLT) of the European Southern Observatory (ESO) at Paranal, Chile. MUSE is an Integral Field Unit (IFU). MUSE works by separating the full field of view ($1' \times 1'$) into 24 sub-fields (2.5" $\times$ 60"). Each of these sub-fields is then processed by 24 identical but independent IFU. Each IFU consists of an image slicer, a spectrograph and a CCD. Each IFU illuminates a 4k $\times$ 4k CCD after slicing the light into 48 slit-like slices (with size $\sim$ 15" $\times\, 0\farcs2$), and decomposing it via a volume phase holographic grating (Barden et al., 1998). The grating achieves a spectral resolution of 1750 at 4650 Å to 3750 at 9300 Å. The data from the 1152 slices is then reconstructed into a $1' \times 1'$ datacube (two spatial axes and one wavelength axis) with a $0\farcs2$ spatial resolution covering from 4750 Å to 9350 Å sampled at 1.25 Å (Bacon et al., 2010).

NGC 6397 was observed during the third commissioning period (ESO Programme ID 60.A-9100(C) Bacon et al., 2014). The observations were taken from July 26th to August 3rd, 2014. The observations covered the central part of NGC 6397 ($\sim 3\farcm5$ from the cluster center see; Fig 2.1). The dataset consists of 23 different pointings of MUSE with short exposure times ranging from 25-60 seconds. In total they obtained 127 exposures of the 23 different $1' \times 1'$ regions (see Fig 2.1). This gives a total integration time of 95 minutes for all the observed part of the cluster.

2.2 Processed and Raw data

The primary goal of the MUSE observation of NGC 6397 was to create the first comprehensive Hertzsprung-Russell diagram with a sample of over 12000 spectra (Husser et al., 2016). The large number of spectra obtained allowed them to study the kinematics of the globular cluster with the goal to probe the presence of a central black hole in the cluster (Kamann et al., 2016). This data is publicly available thought the *MUSE Science Web Service*[1]. The website contains advanced science products such as reduced datacubes, source catalogs and software tools. For NGC 6397, the spectra of the stars in the globular cluster NGC 6397 as published in the studies mentioned above (Husser et al., 2016 and Kamann et al., 2016) are provided. They provided all the obtained spectra with a signal-to-noise ratio of five or larger, i.e. 14 271 spectra in total. For our goal to study the CVs in the globular clusters the published spectra were not enough as they mainly cover the range from main sequence to the tip of the red giant branch[2]. Our approach in this project was to work with the raw science data. The science data can be obtained from the ESO Science Archive Facility. As stated in the ESO Data Access Policy[3], all science data is made publicly available through the science archive after the proprietary period (normally one year after the data have been made available to the principal investigator) and all calibration data are public immediately after the observations.

[1] `http://muse-vlt.eu/science/`

[2] The red giant branch phase is the stage of stellar evolution that follows the main sequence for low to intermediate-mass stars. During this phase the stellar atmosphere expands and the helium core contracts. This phase precedes the Helium burning phase.

[3] `http://archive.eso.org/cms/eso-data-access-policy.html`

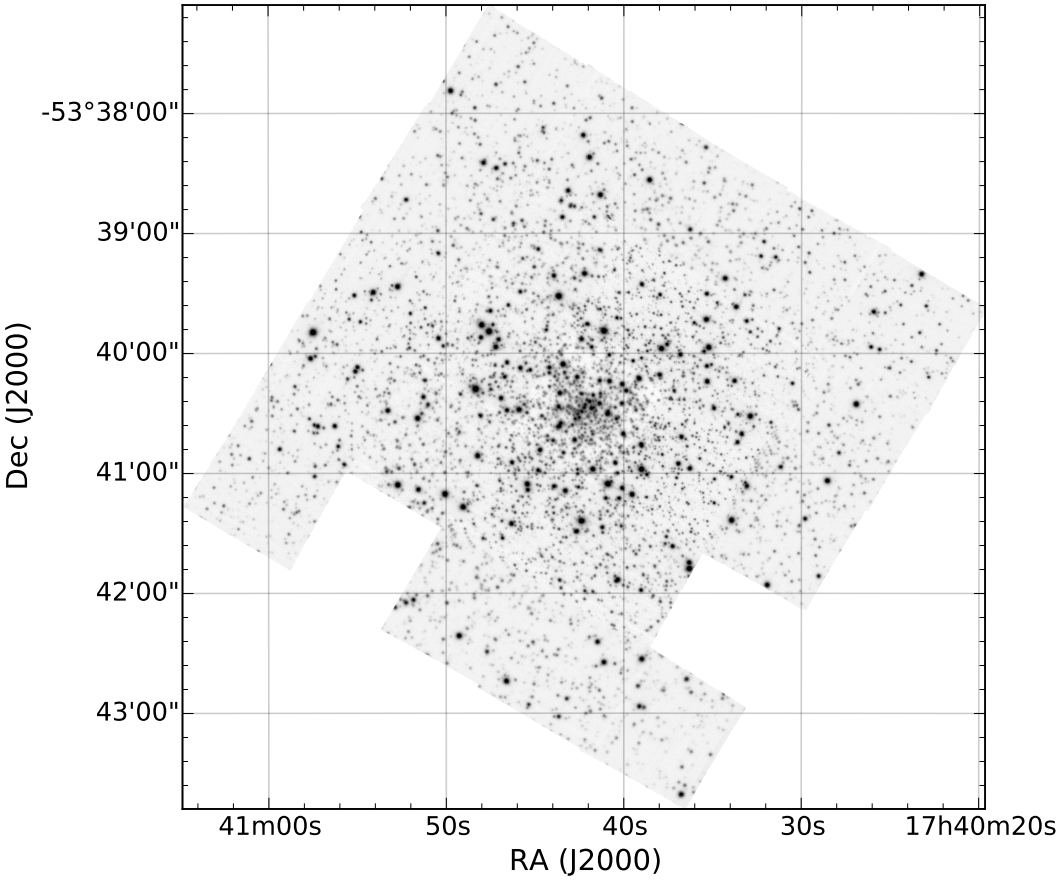

Figure 2.1: White image mosaic of MUSE data cubes of NGC 6397.

2.2.1 Data Reduction

I reduced the data with version 1.2.1 of the MUSE Instrument Pipeline Recipes[4](Weilbacher et al., 2012). The pipeline distribution kit includes several packages. The ones used for this work are the following:

- The Common Pipeline Library version 6.6 (McKay et al., 2004)
- The ESO Recipe Execution Tool (EsoRex)[5] version 3.12.

All the data reduction was done calling *EsoRex* to execute the MUSE DRS recipes from a bash (version 4.3.11) script[6] (alternatively this can be done via the Python bindings, Streicher & Weilbacher (2012)). We summarize the main steps to produce the fully reduced data cube from the raw science and calibration data download from the ESO Science Archive MUSE Query Form. The data reduction steps can be divided into two categories, pre-processing and post-processing. The pre-processing includes all the necessary calibration to remove the instrument signature on the exposures. In the post-processing then the resulting

[4]The MUSE pipeline can be found at `http://www.eso.org/sci/software/pipelines/muse/`

[5]EsoRex is written by the CPL group (Pipeline System Department) European Southern Observatory `http://www.eso.org/sci/software/cpl/esorex.html`

[6]All the configuration files for each of the MUSE recipes used, the bash scripts I wrote, useful python (Python 2.7.6) scripts, the scripts and data for all the plots produced and other text files generated during this internship relevant for the data reduction can be found at `https://github.com/manuelmarcano22/muse2016`

pixel table for each science observation is calibrated for flux and astrometry, and then resampled into a data cube.

1. Pre-processing

   I **Bias subtraction**: Bias subtraction was done by combining 10 different bias images into one master bias file. The combination was done using the sigma clipping technique. Other possible options are combining using the median or average method. Each bias is part of the calibration files taken by ESO every night. A bias frame is dark image with no exposure time taken to account for the read out noise. (Recipe called *muse_ bias*). For this and all subsequent steps we used a table of additional bad pixels of the CCDs created for the MUSE commission runs. This bad pixel table is distributed along with the MUSE pipeline files.

   II **Flat-fielding**: For the flat-field correction 10 individual flat frames were combined into a master flat frame (using the sigma clipping technique). The flat-field images are taking daily at the VLT as part of the standard calibration plan. The master flat contains the combined pixel values of the raw flat exposures. The purpose is to correct for uneven detector sensitivity. The recipe used was *muse_ flat*. Besides the master flat, the recipe also produces a *trace table* containing polynomials defining the location of the slices on the CCD.

   III **Wavelength calibration**: For the wavelength calibration, 15 different arc lamp exposures were used. These are 3 per lamp (Ne, Xe, HgCd lamps). The recipe used is *muse_ wavecal*. It detects arc emission lines and determine the wavelength solution for each slice. The goal is to establish the pixel to wavelength equivalence with high precision.

   IV **Line Spread Function**: The line-spread function is calculated with the recipe *muse_ lsf*. The lines spread function describes the broadening of spectral lines on a CCD. The recipe calculates this wavelength dependent function from 15 arc lamp exposures, and the wavelength solution calculated in the step above.

   V **Geometrical calibration**: In this step, the recipe *muse_ geometry* computes relative location of the slices within the field of view and measures the instrumental point spread function on the detectors. This creates a geometry table. A geometry table comes with the standard MUSE pipeline package as a static calibration file. The geometry table prepared for the third commissioning period was used in reducing the data.

   VI **Illumination Correction**: Flat-fields from the sky or twilight flats are taken weekly at the VLT. These are use to do large scale illumination correction. For the illumination correction also a special purpose illumination flat field called ILLUM can be used as an input to the recipe. These are taken throughout the observing night. We use the one taken closest in time to the science data. Both twilight flats and the ILLUM were used as input to the recipe *muse_ twilight*.

   VII **Pixel table creation**: This step removes all the instrumental signatures on the science exposures and converts them from an image to a large table (called a pixel-table). After calling the recipe *muse_ scibasic*, for each science frame a pixel table is created. The recipe uses the calibration files produced before (master bias, master flat, geometry table, bad pixel table, twilight correction). These tables are the input frames in the subsequent post-processing phase.

2. Post-processing

   I **Flux calibration**: In this step a flux response curve from a standard star exposure is created. The end product of the *muse_ standard* are tables with the response curve as derived from the standard star and the telluric absorption.

II **Sky subtraction**: This step is only needed if the observed object fills the field of view. In the case of the NGC 6397 observation, a reasonable sky spectrum can be obtained on the observation itself and used to substract the sky.

III **Astrometry**: An astrometry solution was done by the MUSE consortium for the third commissioning period. The astrometry solution comes with the MUSE pipeline and was the one used for the data astrometry correction.

IV **Cube assembly**: In this last part, a full data cube is created from a single exposure, the sky background is removed and the flux and the astrometric calibration are applied. In this step the cubes are sampled to a common value ($0\farcs2 \times 0\farcs2 \times 1.25$ Å). Individual data cubes from single exposures can be merged into a single data cube. This was done for each of the 23 different region of the cluster observed. For the center regions, data cubes for the individual exposures were also created.

2.2.2 Spectral extraction and analysis

The spectral subtraction and analysis was carried out with a number of open-source scientific software. To visualize the data cubes and extract the spectra for analysis, QFitsView[7] was used. This is the graphical front-end written QT library of the DPUSER language. Spectral analysis and fitting was done with IRAF (Tody, 1986) (mainly through the command language based on Python PyRAF[8]) and Astropy (Astropy Collaboration et al., 2013). To calculate magnitudes the package Astrolib PySynphot (pysynphot) from the Space Telescope Science Institute was used (Lim et al., 2015) and for plotting we made use of the APLpy package, an open-source plotting package for Python hosted at http://aplpy.github.com

[7] `http://www.mpe.mpg.de/~ott/QFitsView/`

[8] PyRAF is a product of the Space Telescope Science Institute operated for NASA by AURA

Chapter 3: Results

3.1 Cataclysmic Variables

From the population of known CV candidates in NGC 6397, we were able to get the spectra of five of them (see Figure 3.1). In addition to recovering 3 of the previously identified cataclysmic variables, we have obtained the spectra for the first time of two CV candidates (U10 and U22 see figures 3.2 and 3.3). Their spectra confirm that these star are CVs, as suggested by their X-ray data (Grindlay et al., 2001). All the extracted spectra show the most common spectral lines detected from CVs. The most noticeable feature present in all the spectra are the Balmer lines. These are a set of spectral line emissions of the hydrogen atom. In the MUSE spectral range the Hα (6562 Å) and Hβ (4861 Å) lines are detectable. These lines are known to show a double-peaked profile, characteristic of an accretion disc. The red and blue peaks are formed by the emission from the receding and approaching parts of the edge of an accretion disk. With the exception of U10, all the obtained spectra lie within a distance of 11" from the cluster center. Their spectra is obtained from two observing nights of the cluster center. The total exposure time is 340 seconds from a total of 8 different exposures (4×25 s and 4×60 s). U10 lies at a distance of $1.21'$ and was also observed during two different nights. The total exposure time on U10 is 265 seconds divided in 9 short exposures (5×25 s and 4×35 s).

Edmonds et al. (1999) has carefully compared the disks and He ii line ratios of CVs 1–4 with those of other cataclysmic systems. We refer the interested reader to that careful and exhaustive analysis, simply quoting here Edmonds et al.'s conclusions regarding CVs 1–3:

U22 and U17 based on X-ray data.

Same observed for . With absroption H beta for U22.

3.1.1 Variability

From the extracted CV spectra, we calculated the magnitudes in the R band (in the VEGA system), and compare it to the magnitude seen in 2010 by the Hubble space telescope as reported by Cohn et al. (2010). The results are summarized in Table 3.1. The CVs show moderate amplitude variability between the two observing times. This suggests that the majority of the CVs were observed during quiescence and not during an outburst. For some CVs like U22 where the change magnitude is bigger, but still also consistent with no variavirility, the possibility of being observed during outburst is not ruled out. A dwarf nova eruption can result in moderate magnitude changes of ~ 2. This has been observed for U17 and U19. They have been reported to undergo dwarf nova eruptions with amplitudes of 1.8 and 2.7 magnitudes (Shara et al., 2005).

Table 3.1: Magnitudes in the R band for the 5 CVs detected by MUSE in 2014 and the R magnitudes in 2010 studied by Cohn et al. (2010). Some CVs show small magnitude variability between the two epochs (~ 1 magnitude).

CV	**R Magnitude (2014)**	**R $\pm$0.002 (Cohn et al. 2010)**	**Variability**
U17	20.12 ± 0.3	18.52	Yes ($> 3\sigma$)
U23	19.15 ± 0.5	17.88	Marginal $\sim 2.7\sigma$
U10	20.7 ± 1	19.14	No ($< 2\sigma$)
U21	19.79 ± 0.3	19.82	No
U22	18.54 ± 0.9	20.15	No ($< 2\sigma$)

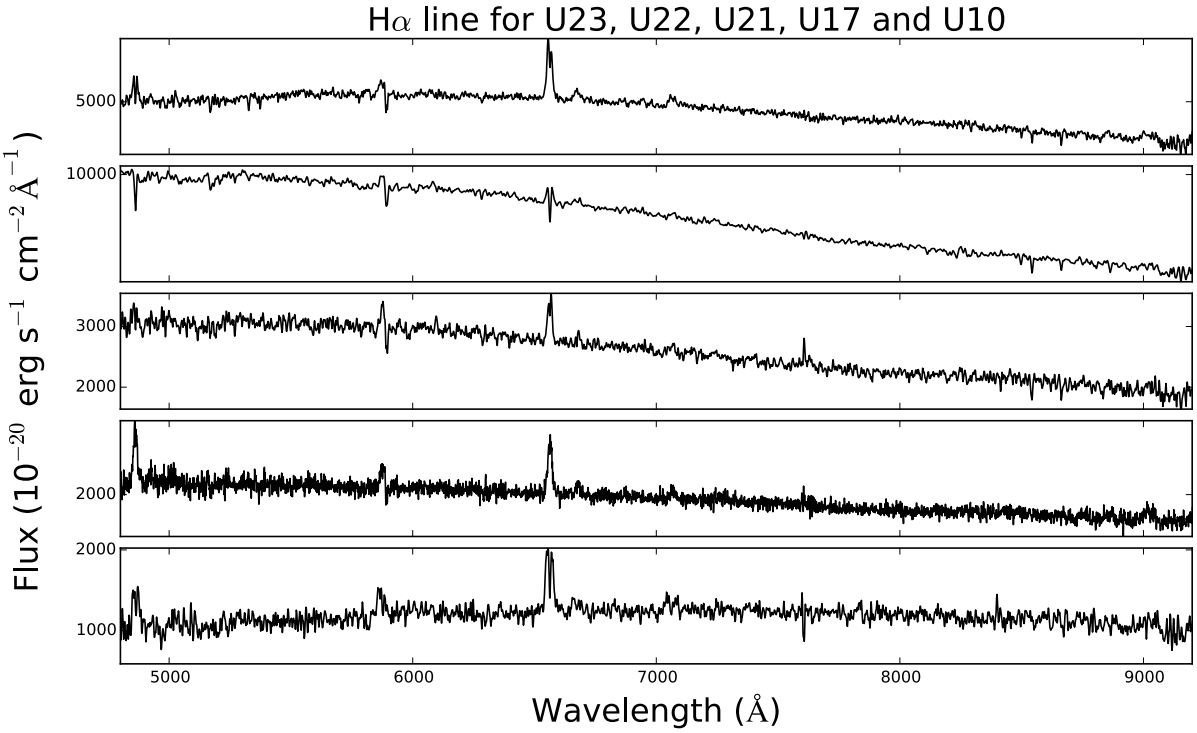

Figure 3.1: Obtained spectra from CVs in NGC 6397. Three of them have been previously identified as CVs: U23, U21 and U17 (Grindlay et al., 1995; Edmonds et al., 1999). U22 and U10 were CV candidates that we confirmed with spectroscopy for the first time. All CVs show strong Balmer lines (Hα 6563 and Hβ 4861 Å). The IDs are from Bogdanov et al. (2010).

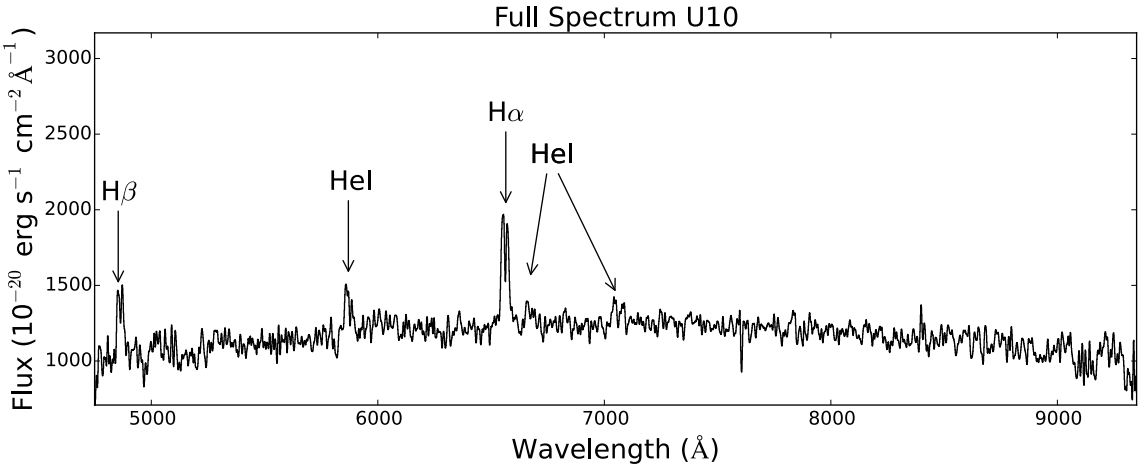

Figure 3.2: Spectrum of U23 with strong Hydrogen double peaked emission (characteristic of an accretion disk), and strong Helium I lines.

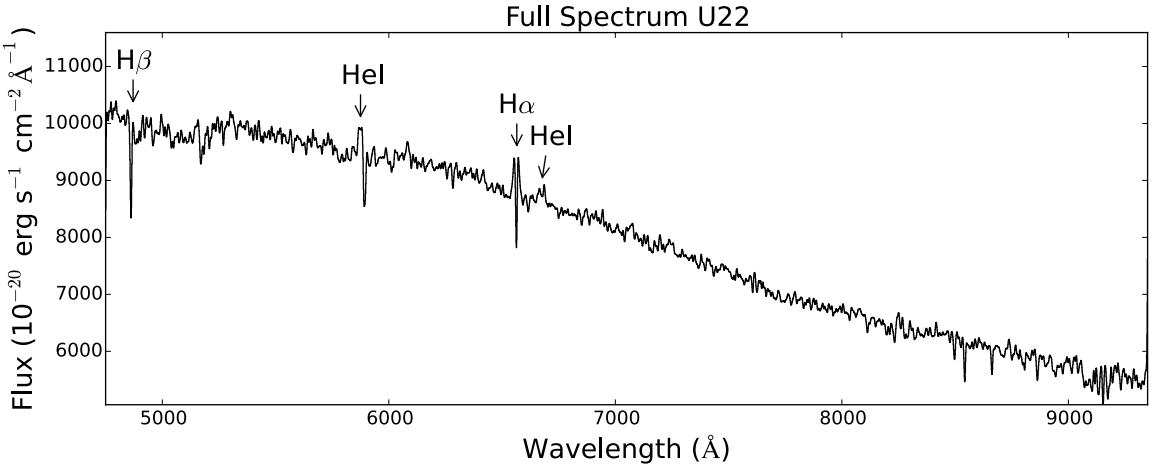

Figure 3.3: Spectrum of U22 with strong Hα double peaked emission, absorption in the Hβ line, and Helium I lines.

3.1.2 Mass ratio

As seen in Figure 3.1, a common feature in all of the extracted spectra is the presence of the Balmer lines. We pay special attention to the $H\alpha$ when it is double peaked (see Figure 3.4). As shown in Casares (2016), we can use the ratio of the double-peak separation (DP) to the full width half maximum (FWHM) of the Hα emission line to get the mass ratio of the companion star to the compact object, q. This was done for CVs U23, U21 and U10 and the results are shown in Figure 3.5.

3.1.3 Radial Velocity

With the 8 different exposures of the center region and the strong Hα line emission the radial velocity evolution of the CV can be traced. This is done by employing the cross-correlation algorithms of Tonry & Davis (1979), as implemented in the IRAF Radial Velocity Analysis Package. This was done for U23, one of the brightest and one of the only two CVs in NGC 6397 for which the orbital period has been measured (Kaluzny & Thompson, 2003). The first exposure of 25 second for the first night was used as the reference to calculate radial velocity shifts. No significant radial velocity was detected between each individual short exposure. The same procedure to determine the radial velocity shift between the combined exposures for the first night and for the second observing night. We obtained an estimate of 23.4 ± 14 km/s, which is not significant enough to claim a detected RV variation.

3.2 Low-mass X-ray Binary

Besides the population of CVs in NGC 6397 we also studied a LMXB located near the center in NGC 6397. The goal was to detect possible Hα emmision from the LMXB. The detection of hydrogen lines in the LMXB will remove any ambiguities regarding the composition of the neutron star atmosphere. The absence of hydrogen would be an argument for using a Helium atmosphere model resulting different mass-radius relations than for a hydrogen model. This will help better constrain the equation of state of neutron stars (see Section 1.2.2). Using all the available observations of the center, we estimated the flux in the Hα band to be 8.2×10^{-18} erg/s/cm^2. This is a very faint object (R magnitude of ~ 26, Heinke et al. (2014)). Longer integration time is needed to be able to obtain a spectra with a good signal-to-noise ratio and study the spectra of the LMXB.

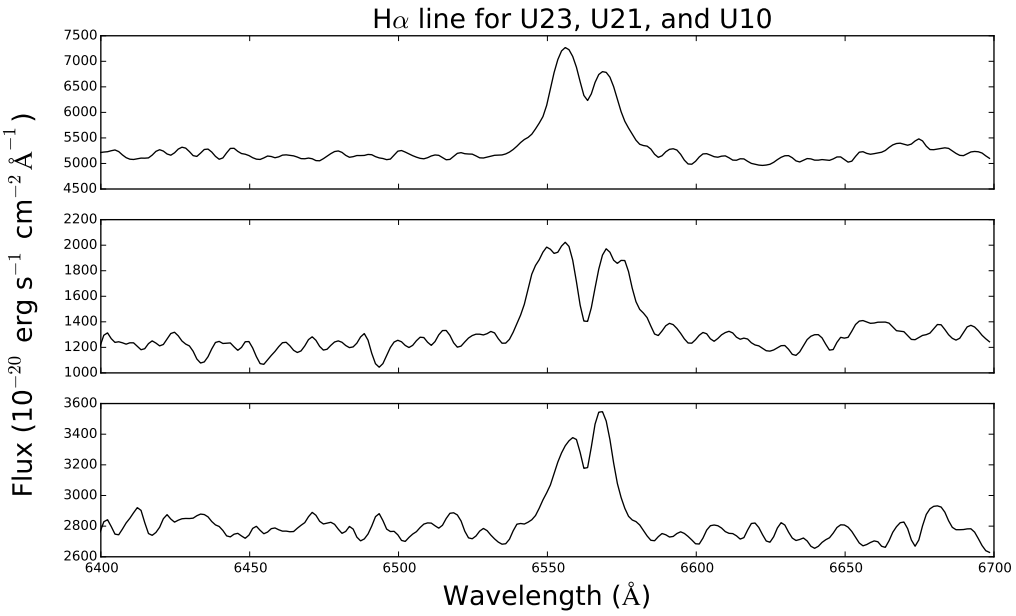

Figure 3.4: Zoom of the spectra around Hα for U23 (top), U21 (middle), and U10 (bottom)

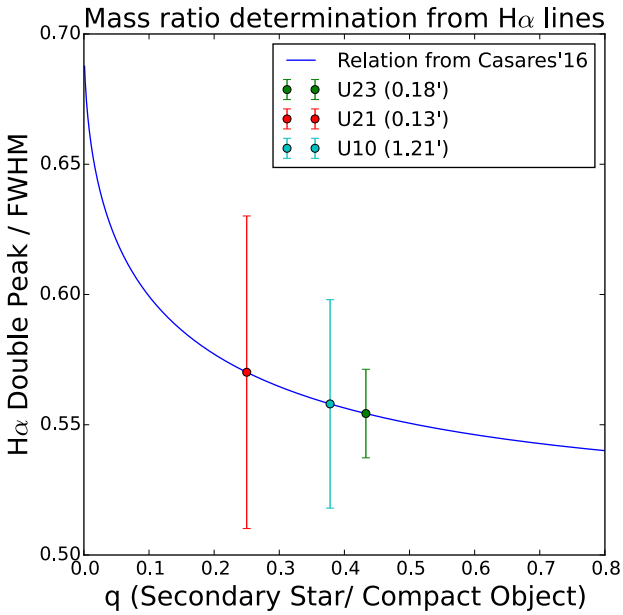

Figure 3.5: The solid line is the relation between the ratio of Hα double peak separation to Full width at half maximum (FWHM) and the mass ratio q (companion star mass over white dwarf mass) from Casares (2016). Our measured values for the CVs are shown as points with their error bars. The values in parenthesis are the projected distance to the cluster center for each CV. The value of q for U23 is 0.433, for U21 is 0.25 and 0.3 for U10.

Chapter 4: Discussion and Conclusions

To finish we come back to the four open questions about CVs in globular clusters discussed in the introduction.

4.1 Primordial CVs

In this work, we studied the population of CVs in NGC 6397. Previous photometric and X-ray studies of this cluster have identified a sample of 15 CV candidates. In this work we located the candidates on the MUSE observations to examine their spectral signature and extend the sample of 6 to 8 spectroscopically confirmed CV candidates. From the sample, we were able to unambiguously identify 5 CVs via their bright Hα line in emission, sign of an accretion disk. We have obtained the spectra of two new CVs, one of the spectra being the first one from a CV outside the cluster center. Increasing the sample size of CV spectra, and looking at the CVs in different locations in the cluster, increases the chances of detecting the predicted populations of CVs. For the CV candidates farther from the cluster center (with one exception), no Hα line was detected. This suggest that these might belong to a different kind of 'faint' CV population. Their radial distribution and their undetected Hα emission might suggest that these are primordial CVs. CVs from primordial origins are expected to be near the minimum period and have their optical spectra dominated by the white dwarf as the companion has lost most of its mass to the white dwarf. Hydrogen emission is still expected but probably weakened and inside broad absorption lines, the signature of a white dwarf. The lack of bright hydrogen lines from these object also leaves the door open to the possibility that the white dwarfs are accreting from a helium dwarf companion. These are of great interest as gravitational waves sources for future missions like eLISA (Amaro-Seoane et al., 2012). Such types of CVs have never been identify in globular clusters although they are predicted to exist. Deeper observation with MUSE are needed to get spectra with sufficient signal-to-noise ratio and correctly classify them as such.

Studying the companion stars of the CVs can also provide information about primordial CVs, as dynamically formed CVs are expected to have a bias towards having a more massive companions. None of the obtained spectra show the signature of an M star (TiO lines e.g Marsh 1990). This suggest that the companion stars might possibly be a K type star ($0.54 - 0.9 M_\odot$, Gray 2005). Knowing that the turnoff mass[1] is $0.77 M_\odot$ for NGC 6397 (De Marco et al., 2005), this gives us a range of $\sim 0.5 - 0.8 M_\odot$, leaving the possibility for the companion to be either a M type star or even a low mass white dwarf or helium dwarf.

4.2 Periods

The Hα emission line was used to detect radial velocity variations in the CVs. Since the period of U23 is known, we used it as a check if radial velocity could be detected in the short exposures taken by MUSE. However, since the method significantly depends on the strength of the emission line (and the integration time required to detect it), the short exposures available were not enough to be able to unambiguously detect radial velocity shifts. This suggests that longer integration time (> 25 seconds) is needed to be able to determine the period of the CVs in NGC 6397 with the MUSE instrument. Exposures of a few minutes (~ 6 m) with the data on two different nights combined allowed us to detect the radial velocity shift. With longer exposures of globular clusters, MUSE would be able to trace simultaneously the radial

[1] the turn off mass is the maximum mass on the main sequence. This can serve as a rough estimate of the maximum mass of main sequence stars in a globular clusters.

velocity shift of multiple objects and determine the orbital parameters of binaries in globular clusters. This is of great interest as the number of CVs with known periods in globular clusters is very low.

4.3 Magnetism and dwarf novae

It has been proposed that the majority of CVs in globular clusters are magnetic (Grindlay, 1999). For NGC 6397, remarkably, all 4 previously spectrally confirmed CVs show prominent Helium II lines. These line are generally associated with magnetic and nova-like CVs (Echevarria, 1988). We did not detect any Helium II line in any of the two newly studied spectra (U10 and U22). This might suggest that they are not magnetic in nature. However, this is not conclusive as the strongest He II line is outside of the MUSE spectral range (4686 Å). This means that the possibility that the two newly identified CVs are magnetic have not been completely ruled out.

Regarding the dwarf novae, U22 showed a moderate increase in brightness compared to previous observations. Based on data from dwarf novae in the field we can estimate how likely it is that we have detected a CV during an outburst. About half of all known fields CVs are dwarf novae ($\sim$ 40%) and most discovered undergo 2-5 mag outburst (Downes et al., 2001; Warner, 2003). With data from the AAVSO catalog with a sample of 21 field DNs studied for an interval of three years Szkody & Mattei (1984) concluded that the probability of a DN being in quiescence at a random epoch is $\sim$ 85%. Due to the close distance to NGC 6397 we can make the assumption that we would have detected any outburst during the MUSE observation of the cluster. Based on this assumption, we should have detected $\sim$ 15% of the DN in NGC 6397. Even if we limit our sample size of potential DN to the 15 candidates, we expect to see at least 1 CV in outburst during the observation. There are many caveats with the assumptions made as the estimated rates of DN are mainly empirical and can suffer from selection biases due to the fact that observations of bright and long period outbursts are easier to detect.

More like U17 or U22 the change cannot be consluseive as the error in the flux is higer and U23. U17 have been shown to be a draf novaeo

For CV2 was also the case in http://adsabs.harvard.edu/abs/2006MNRAS.365..548K kalyzny CV3 also mentioned. CV2 is U19 we could nsee.

CV3 is U17.

This is not irrefutable evidence that U22 was observed during an outburst and photometric follow up to study the variability is needed for confirmation. If U22 is indeed a dwarf novae it would be the third one identified in NGC 6397 (Shara et al., 2005) and contributes to the still small sample of DN outburst spectra (37 out of 1600 CVs, Downes et al. 2001). The fact that only one possible DN in outburst was identified supports the claim made by Shara et al. (1996) that DNs are very rare in globular clusters, maybe due to the fact that the majority are magnetic and thus are less likely to undergo DN outbursts.

Chapter 5: Future Work

Altogether we have demonstrated how an IFU like MUSE can be used to efficiently study the population of compact objects in globular clusters. Here, we exposed some hints that the population of field CVs and CVs in GCs are different. This is due to the fact that the dynamics of the whole globular cluster plays a role in the formation of these compact objects. Deeper observations at different epochs (with separation of $\lesssim$ 10hrs) are needed to constrain the current models on the evolution of globular clusters and formation of binaries in them. MUSE is a well adapted instrument for the task as it allows us to study the variability and spectral features of a high number of objects simultaneously. This opens the way for the discovery of new objects in globular clusters. For this work we were limited by the very short exposure times. This is mainly because these observations took place during the commissioning period and so they were constrained by the overall commission goals. MUSE is now in regular observation time and among its future and current targets there are a number of other galactic globular cluster. Also improvements in the instrument are expected soon, like for example the use of adaptive optic and narrow field mode. This means a vast number of new data sets that can be exploited to improve our understanding on the formation of compact objects in globular clusters.

5.1 Follow up Observation

We have requested deep observations to detect the hydrogen line and deduct the nature of the atmosphere of the NS in the LMXB in the center of NGC 6397. This will allow us to use the correct models to model the X-ray spectra and make constraints on the neutron star equation of state. Further, if we can detect radial velocity motion, we can obtain independent constraints on the neutron star mass, one of the free parameters in the spectral modeling, and therefore obtain more precise constraints on the equation of state.

Since MUSE has a big field of view and the LMXB is close to the cluster center, the observation will also allow us to study the CV population in the core of NGC 6397. As a secondary objective, the proposed long exposure will allow a much deeper study of the sources in the cluster core.

5.2 Data analysis

5.2.1 Optimal Spectra Extraction

The spectral extraction was done with QFitsView by adding the spectra from four adjacent pixels from the identified source in the datacube. QFitView allows to vary the number of pixels to add, and to obtain the spectra from the mean or median of the selected number of adjacent pixels. The number of pixels to add was determined by visual examination of the spectra. An optimal way was shown by Horne & Marsh (1986). This could potentially increase the quality of the extracted spectra.

5.2.2 Short Term variability

Besides the radial velocity shift with the individual short exposures, we can examine the short term variability of the CVs. This can be done for the sources bright enough to be detected in the short 25 seconds exposures. We plan to study the variations in the flux of strong emission lines like the Hα line. This can help us determine the magnetic nature of the CVs, as magnetic CVs are expected to be more variable in short timescales.

5.2.3 Processed data

The data for over 14 000 extracted spectra from the MUSE observation of NGC 6397 is available online. This only includes the extracted spectra with SNR > 5 and mainly includes main sequence stars, but a thoroughly search can be done to identify possible binaries in the data set. The plan would be to examine the data set looking for strong Hα emitters as signs of an accretion disk. They can be identified by measuring the ratio of the flux from the spectra continuum to the flux from the Hα lines for each available spectra. Searching for a flux ratio above a certain value can help us identify possible compact object candidates in the available processed data set.

5.3 Reproducibility

5.3.1 Continuous Analysis

Being able to replicate and validate previous results is in the heart of science. One way of ensuring reproducibility in research areas involving computer analyses is creating an isolated computational environment that captures the versions and dependencies of all used libraries and programs. Dockers[1] containers are a open source alternative that provides a fast and lightweight way to isolated the computational environment in which data reduction and analysis was done. This avoids any future dependencies or versions conflicts and allows the work to be portable and easily reproduced for validation or improvements in any operating system. Recently the termed 'continuous analysis' was introduced for container-based research flows if they include version control and specially continuous integration, a well established software development technique. The details are outlined in Beaulieu-Jones & Greene (2016). The plan is to adopt such workflows for future work.

5.3.2 Cloud Computing

Another challenge for astronomical data that applies for MUSE data is how computationally demanding their processing can be. For example, the recommended memory for a machine for creating the final data cube from a single MUSE observation and the required set of calibrations is 64 GB of memory. The same applies for the number of CPU cores and disk space. This is why the data reduction work was done in a institutional server with the minimum requirements. This is not optimal for portability and reproducibility. One option is to make use of a cloud computing environment, such as provided by the Amazon Web Service (AWS) that provide on-demand access to large-scale computational resources. An example of something like this done in science for reproducibility goals is the work of Ragan-Kelley et al. (2013). More recently in astrophysics this approach have been explored by members of the Square Kilometer Array organization and members of the project CHILES, see Dodson et al. (2016) for the details. In the future this cloud computing approach can be adopted to the processing of MUSE data and give access to the configuration files of the created Amazon Web Service instance created for the data reduction and analysis.

[1] `https://www.docker.com/`

Bibliography

Amaro-Seoane, P., Aoudia, S., Babak, S., Binétruy, P., Berti, E., Bohé, A., Caprini, C., Colpi, M., Cornish, N. J., Danzmann, K., Dufaux, J.-F., Gair, J., Jennrich, O., Jetzer, P., Klein, A., Lang, R. N., Lobo, A., Littenberg, T., McWilliams, S. T., Nelemans, G., Petiteau, A., Porter, E. K., Schutz, B. F., Sesana, A., Stebbins, R., Sumner, T., Vallisneri, M., Vitale, S., Volonteri, M., & Ward, H. 2012, Classical and Quantum Gravity, 29, 124016

Antonov, V. A. 1962, Solution of the problem of stability of stellar system Emden's density law and the spherical distribution of velocities

Astropy Collaboration, Robitaille, T. P., Tollerud, E. J., Greenfield, P., Droettboom, M., Bray, E., Aldcroft, T., Davis, M., Ginsburg, A., Price-Whelan, A. M., Kerzendorf, W. E., Conley, A., Crighton, N., Barbary, K., Muna, D., Ferguson, H., Grollier, F., Parikh, M. M., Nair, P. H., Unther, H. M., Deil, C., Woillez, J., Conseil, S., Kramer, R., Turner, J. E. H., Singer, L., Fox, R., Weaver, B. A., Zabalza, V., Edwards, Z. I., Azalee Bostroem, K., Burke, D. J., Casey, A. R., Crawford, S. M., Dencheva, N., Ely, J., Jenness, T., Labrie, K., Lim, P. L., Pierfederici, F., Pontzen, A., Ptak, A., Refsdal, B., Servillat, M., & Streicher, O. 2013, Astronomy and Astrophysics, 558, A33

Bacon, R., Accardo, M., Adjali, L., Anwand, H., Bauer, S., Biswas, I., Blaizot, J., Boudon, D., Brau-Nogue, S., Brinchmann, J., Caillier, P., Capoani, L., Carollo, C. M., Contini, T., Couderc, P., Daguisé, E., Deiries, S., Delabre, B., Dreizler, S., Dubois, J., Dupieux, M., Dupuy, C., Emsellem, E., Fechner, T., Fleischmann, A., François, M., Gallou, G., Gharsa, T., Glindemann, A., Gojak, D., Guiderdoni, B., Hansali, G., Hahn, T., Jarno, A., Kelz, A., Koehler, C., Kosmalski, J., Laurent, F., Le Floch, M., Lilly, S. J., Lizon, J.-L., Loupias, M., Manescau, A., Monstein, C., Nicklas, H., Olaya, J.-C., Pares, L., Pasquini, L., Pécontal-Rousset, A., Pelló, R., Petit, C., Popow, E., Reiss, R., Remillieux, A., Renault, E., Roth, M., Rupprecht, G., Serre, D., Schaye, J., Soucail, G., Steinmetz, M., Streicher, O., Stuik, R., Valentin, H., Vernet, J., Weilbacher, P., Wisotzki, L., & Yerle, N. 2010, in Proceedings of the SPIE, Vol. 7735, Ground-based and Airborne Instrumentation for Astronomy III, 773508

Bacon, R., Vernet, J., Borisova, E., Bouche, N., Brinchmann, J., Carollo, M., Carton, D., Caruana, J., Cerda, S., Contini, T., Franx, M., Girard, M., Guerou, A., Haddad, N., Hau, G., Herenz, C., Herrera, J. C., Husemann, B., Husser, T.-O., Jarno, A., Kamann, S., Krajnovic, D., Lilly, S., Mainieri, V., Martinsson, T., Palsa, R., Patricio, V., Pecontal, A., Pello, R., Piqueras, L., Richard, J., Sandin, C., Schroetter, I., Selman, F., Shirazi, M., Smette, A., Soto, K., Streicher, O., Urrutia, T., Weilbacher, P., Wisotzki, L., & Zins, G. 2014, The Messenger, 157, 13

Balman, S. 2012, Memorie della Societa Astronomica Italiana, 83, 585

Barden, S. C., Arns, J. A., & Colburn, W. S. 1998, in Proceedings of the SPIE, Vol. 3355, Optical Astronomical Instrumentation, ed. S. D'Odorico, 866–876

Beaulieu-Jones, B. K. & Greene, C. S. 2016, bioRxiv

Bogdanov, S., Berg, M. v. d., Heinke, C. O., Cohn, H. N., Lugger, P. M., & Grindlay, J. E. 2010, The Astrophysical Journal, 709, 241

Brown, G., Lee, C.-H., Wijers, R., & Bethe, H. 2000, Physics Reports, 333-334, 471

Cannizzo, J. K. & Mattei, J. A. 1998, The Astrophysical Journal, 505, 344

Casares, J. 2016, The Astrophysical Journal, 822, 99

Chandrasekhar, S. 1931, The Astrophysical Journal, 74, 81

Cohn, H. N., Lugger, P. M., Couch, S. M., Anderson, J., Cool, A. M., van den Berg, M., Bogdanov, S., Heinke, C. O., & Grindlay, J. E. 2010, The Astrophysical Journal, 722, 20

Cool, A. M., Grindlay, J. E., Cohn, H. N., Lugger, P. M., & Slavin, S. D. 1995, The Astrophysical Journal, 439, 695

Cool, A. M., Grindlay, J. E., Krockenberger, M., & Bailyn, C. D. 1993, The Astrophysical Journal Letters, 410, L103

Coppejans, D. L., Körding, E. G., Miller-Jones, J. C. A., Rupen, M. P., Knigge, C., Sivakoff, G. R., & Groot, P. J. 2015, Monthly Notices of the Royal Astronomical Society, 451, 3801

Cropper, M. 1990, Space Science Reviews, 54

de Boer, K. & Seggewiss, W. 2008, Stars and Stellar Evolution (EDP Sciences)

De Loore, C. W. H. & Doom, C. 1992, Astrophysics and Space Science Library, Vol. 179, Structure and Evolution of Single and Binary Stars (Dordrecht: Springer Netherlands)

De Marco, O., Shara, M. M., Zurek, D., Ouellette, J. A., Lanz, T., Saffer, R. A., & Sepinsky, J. F. 2005, The Astrophysical Journal, 632, 894

Demorest, P. B., Pennucci, T., Ransom, S. M., Roberts, M. S. E., & Hessels, J. W. T. 2010, Nature, 467, 1081

Dodson, R., Vinsen, K., Wu, C., Popping, A., Meyer, M., Wicenec, A., Quinn, P., van Gorkom, J., & Momjian, E. 2016, Astronomy and Computing, 14, 8

Downes, R. A., Webbink, R. F., Shara, M. M., Ritter, H., Kolb, U., & Duerbeck, H. W. 2001, The Publications of the Astronomical Society of the Pacific, 113, 764

Duncan, R. C. & Thompson, C. 1992, The Astrophysical Journal, 392, L9

Echevarria, J. 1988, Monthly Notices of the Royal Astronomical Society, 233, 513

Edmonds, P. D., Grindlay, J. E., Cool, A., Cohn, H., Lugger, P., & Bailyn, C. 1999, The Astrophysical Journal, 516, 250

Fowler, R. H. 1926, Monthly Notices of the Royal Astronomical Society, 87, 114

Frank, J., King, A., & Raine, D. J. 2002, Accretion Power in Astrophysics: Third Edition (Cambridge University Press)

Gehrz, R. D., Truran, J. W., Williams, R. E., & Starrfield, S. 1998, Publications of the Astronomical Society of the Pacific, 110, 3

Gray, D. 2005, The Observation and Analysis of Stellar Photospheres (Cambridge University Press)

Grindlay, J. E. 1999, in Astronomical Society of the Pacific Conference Series, Vol. 157, Annapolis Workshop on Magnetic Cataclysmic Variables, ed. C. Hellier & K. Mukai, 377

Grindlay, J. E. 2006, Advances in Space Research, 38, 2923

Grindlay, J. E., Cool, A. M., Callanan, P. J., Bailyn, C. D., Cohn, H. N., & Lugger, P. M. 1995, The Astrophysical Journal Letters, 455, L47

Grindlay, J. E., Heinke, C. O., Edmonds, P. D., Murray, S. S., & Cool, A. M. 2001, The Astrophysical Journal Letters, 563, L53

Hamada, T. & Salpeter, E. E. 1961, The Astrophysical Journal, 134, 683

Harris, W. E. 1996, The Astronomical Journal, 112, 1487

Heger, A., Fryer, C. L., Woosley, S. E., Langer, N., & Hartmann, D. H. 2003, The Astrophysical Journal, 591, 288

Heinke, C. O., Cohn, H. N., Lugger, P. M., Webb, N. A., Ho, W. C. G., Anderson, J., Campana, S., Bogdanov, S., Haggard, D., Cool, A. M., & Grindlay, J. E. 2014, Monthly Notices of the Royal Astronomical Society,, 444, 443

Hewish, A., Bell, S. J., Pilkington, J. D. H., Scott, P. F., & Collins, R. A. 1968, Nature, 217, 709

Horne, K. & Marsh, T. R. 1986, Monthly Notices of the Royal Astronomical Society, 218, 761

Husser, T.-O., Kamann, S., Dreizler, S., Wendt, M., Wulff, N., Bacon, R., Wisotzki, L., Brinchmann, J., Weilbacher, P. M., Roth, M. M., & Monreal-Ibero, A. 2016, Astronomy and Astrophysics, 588, A148

Hut, P., McMillan, S., Goodman, J., Mateo, M., Phinney, E. S., Pryor, C., Richer, H. B., Verbunt, F., & Weinberg, M. 1992, Publications of the Astronomical Society of the Pacific, 104, 981

Ivanova, N., Belczynski, K., Fregeau, J. M., & Rasio, F. A. 2005, Monthly Notices of the Royal Astronomical Society, 358, 572

Ivanova, N., Heinke, C. O., Rasio, F. A., Taam, R. E., Belczynski, K., & Fregeau, J. 2006, Monthly Notices of the Royal Astronomical Society, 372, 1043

Kaluzny, J. & Thompson, I. B. 2003, The Astronomical Journal, 125, 2534

Kaluzny, J., Thompson, I. B., Krzeminski, W., & Schwarzenberg-Czerny, A. 2006, Monthly Notices of the Royal Astronomical Society, 365, 548

Kamann, S., Husser, T.-O., Brinchmann, J., Emsellem, E., Weilbacher, P. M., Wisotzki, L., Wendt, M., Krajnović, D., Roth, M. M., Bacon, R., & Dreizler, S. 2016, ArXiv e-prints, 1602, arXiv:1602.01643

Kepler, S. O. & Bradley, P. A. 1995, Baltic Astronomy, 4

King, I. R. 1966, The Astronomical Journal, 71, 64

Kinney, A. 1994, in Astronomical Society of the Pacific Conference Series, Vol. 54, The Physics of Active Galaxies, ed. G. V. Bicknell, M. A. Dopita, & P. J. Quinn, 61

Kippenhahn, R., Kohl, K., & Weigert, A. 1967, Zeitschrift fur Astrophysik, 66

Knigge, C. 2012, Memorie della Societa Astronomica Italiana, 83

Koester, D. & Chanmugam, G. 1990, Reports on Progress in Physics, 53, 837

Koester, D. & Weidermann, V. 1980, Astronomy and Astrophysics, 81

Kopal, Z. 1955, Annales d'Astrophysique, 18

—. 1959, Close binary systems (New York: Wiley)

Körding, E., Rupen, M., Knigge, C., Fender, R., Dhawan, V., Templeton, M., & Muxlow, T. 2008, Science, 320, 1318

Krzeminski, W. & Serkowski, K. 1977, The Astrophysical Journal, 216, L45

Lattimer, J. M. & Prakash, M. 2001, The Astrophysical Journal, 550, 426

—. 2007, Physics Reports, 442, 109

Lim, P. L., Diaz, R. I., & Laidler, V. 2015, PySynphot User's Guide, Baltimore, MD:STScI, `http://ssb.stsci.edu/pysynphot/docs/`

Lubow, S. H. & Shu, F. H. 1975, The Astrophysical Journal, 198, 383

Lynden-Bell, D. & Eggleton, P. P. 1980, Monthly Notices of the Royal Astronomical Society, 191, 483

Lynden-Bell, D. & Pringle, J. E. 1974, Monthly Notices of the Royal Astronomical Society, 168, 603

Lynden-Bell, D. & Wood, R. 1968, Monthly Notices of the Royal Astronomical Society, 138, 495

Maccarone, T. & Knigge, C. 2007, Astronomy and Geophysics, 48, 5.12

Madsen, J. 1999, in Hadrons in Dense Matter and Hadrosynthesis, ed. J. Cleymans, H. B. Geyer, & F. G. Scholtz, Vol. 516 (Berlin, Heidelberg: Springer Berlin Heidelberg), 162–203

Marsh, T. R. 1990, Astrophysical Journal, 357, 621

McKay, D. J., Ballester, P., Banse, K., Izzo, C., Jung, Y., Kiesgen, M., Kornweibel, N., Lundin, L. K., Modigliani, A., Palsa, R. M., & Sabet, C. 2004, in Proceedings of the International Society for Optical Engineering, Vol. 5493, Optimizing Scientific Return for Astronomy through Information Technologies, ed. P. J. Quinn & A. Bridger, 444–452

McLaughlin, D. E. & van der Marel, R. P. 2005, The Astrophysical Journal Supplement Series, 161, 304

Meylan, G. & Heggie, D. C. 1997, Astronomy and Astrophysics Reviews, 8, 1

Oppenheimer, J. R. & Volkoff, G. M. 1939, Physical Review, 55, 374

Osaki, Y. 1974, Publications of the Astronomical Society of Japan, 26, 429

Patterson, J. 1994, Publications of the Astronomical Society of the Pacific, 106, 209

Postnov, K. A. & Yungelson, L. R. 2014, Living Reviews in Relativity, 17

Prada Moroni, P. G. & Straniero, O. 2009, Astronomy and Astrophysics, 507, 1575

Ragan-Kelley, B., Walters, W. A., McDonald, D., Riley, J., Granger, B. E., Gonzalez, A., Knight, R., Perez, F., & Caporaso, J. G. 2013, The ISME Journal, 7, 461

Reisenegger, A., Prieto, J., Benguria, R., Lai, D., & Araya, P. 2005, in Magnetic fields in the universe, from laboratory and stars to primordial structures, Angra dos Reis, Brazil, 28 November - 3 December 2004, Vol. 784, 263–273, [,263(2005)]

Rhoades, C. E. & Ruffini, R. 1974, Physical Review Letters, 32, 324

Robinson, E. L. 1983, in Astrophysics and Space Science Library, Vol. 101, IAU Colloq. 72: Cataclysmic Variables and Related Objects, ed. M. Livio & G. Shaviv, 1–14

Schuerman, D. W. 1972, Astrophysics and Space Science, 19, 351

Shara, M. M. 1989, Publications of the Astronomical Society of the Pacific, 101, 5

Shara, M. M., Bergeron, L. E., Gilliland, R. L., Saha, A., & Petro, L. 1996, Astrophysical Journal, 471, 804

Shara, M. M., Hinkley, S., Zurek, D. R., Knigge, C., & Dieball, A. 2005, The Astronomical Journal, 130, 1829

Starrfield, S., Iliadis, C., & Hix, W. R. 2016, Publications of the Astronomical Society of the Pacific, 128, 051001

Streicher, O. & Weilbacher, P. M. 2012, Astronomical Data Analysis Software and Systems XXI, 461

Suh, I.-S. & Mathews, G. J. 2000, The Astrophysical Journal, 530, 949

Szkody, P. & Mattei, J. A. 1984, Publications of the Astronomical Society of the Pacific, 96, 988

Tapia, S. 1977, The Astrophysical Journal, 212, L125

Tauris, T. M. & van den Heuvel, E. P. J. 2006, in Compact stellar X-ray sources, 623–665

Taylor, J. M., Grindlay, J. E., Edmonds, P. D., & Cool, A. M. 2001, The Astrophysical Journal Letters, 553, L169

Tody, D. 1986, in Proceedings of the SPIE, Vol. 627, Instrumentation in astronomy VI, ed. D. L. Crawford, 733

Tonry, J. & Davis, M. 1979, Astronomical Journal, 84, 1511

van den Heuvel, E. P. J. 1976, in IAU Symposium, Vol. 73, Structure and Evolution of Close Binary Systems, ed. P. Eggleton, S. Mitton, & J. Whelan, 35

Verbunt, F. 1982, Space Science Reviews, 32

Verbunt, F., Bunk, W. H., Ritter, H., & Pfeffermann, E. 1997, Astronomy and Astrophysics, 327

Warner, B. 2003, Cataclysmic Variable Stars (Cambridge University Press)

Weilbacher, P. M., Streicher, O., Urrutia, T., Jarno, A., Pécontal-Rousset, A., Bacon, R., & Böhm, P. 2012, in SPIE Astronomical Telescopes+ Instrumentation, International Society for Optics and Photonics, 84510B–84510B

Wickramasinghe, D. T. & Ferrario, L. 2000, Publications of the Astronomical Society of the Pacific, 112, 873

Zavlin, V. E., Pavlov, G. G., & Shibanov, Y. A. 1996, Astronomy and Astrophysics, 315, 141

List of Acronyms

BH Black Hole

CN Classical Novae

CV Cataclysmic Variable

DN Dwarf Nova

EOS Equation of State

ESO European Southern Observatory

FWHM Full Width at Half Maximum

GC Globular Cluster

HMXB High-mass X-Ray Binaries

IFU Integral Field Unit

IP Intermediate Polar

LMXB Low-mass X-ray binary

MS Main Sequence

MUSE Multi Unit Spectroscopic Explorer

NL Novae-like

NS Neutron Star

VLT Very Large Telescope

WD White Dwarf